RSC Advances

ROYAL SOCIETY OF CHEMISTRY

www.rsc.org/advances

Performance of Silicon Rubber Coated Polyetherimide Hollow Fibers for CO_2 Removal via a Membrane Contactor

S.A. Hashemifard[a*], A.F. Ismail[b*], T. Matsuura[b,c], M. Rezaei DashtArzhandi [b]

[a] *Chemical Engineering Department, Engineering Faculty, Persian Gulf University, Bushehr 7516913817, Iran*
[b] *Advanced Membrane Technology Research Centre (AMTEC), Universiti Teknologi Malaysia, 81310 UTM Skudai, Johor Darul Ta'zim, Malaysia*
[c] *Department of Chemical and Biological Engineering, University of Ottawa, 161 Louis Pasteur St., Ottawa, ON, Canada K1N 6N5*

Abstract

This study focuses on the effect of a silicon rubber coating technique on the hollow fiber membrane contactor for the purpose of CO_2 removal. The polymer and the coating agent used were polyetherimide (PEI) and polydimethylsiloxane (PDMS) respectively. The hollow fibers were fabricated via a simple wet spinning technique. The surfaces of the hollow fibers were coated by means of PDMS dissolved in n-hexane applying different protocols. An effort was made to keep the silicon rubber coating layer porous. The membranes were characterized by applying gas permeation test (GPT) via pure helium, critical entry pressure of water (CEPw), contact angle, gas absorption test and scanning electron microscopy (SEM). Based on the observations, the coating technique resulted in drastic changes in the contact angle and CEPw of the coated membranes for the inside and outside coated hollow fiber membranes in common. Disregarding the method of coating and even the polymer concentration, the contact angle has been enhanced dramatically. The CO_2 absorption results revealed that by blowing nitrogen (600 kPa) through the lumen side of the hollow fibers during the PDMS coating process onto the outside surface, the absorption flux of the membranes was increased. A slight decrease in CO_2 absorption flux for the other cases was outweighed by a substantial enhancement in the membrane wetting resistant due to the high contact angle and CEPw. These observations showed the high influence of the silicon rubber layer on the CO_2 gas absorption, which emphasizes the role of this key-parameter in controlling the ultimate membrane contactor performance.

1. Introduction

Aggressive levels of anthropogenic greenhouse gases, primarily carbon dioxide (CO_2), impose irreversible environmental, economic and operational impacts to the earth. Hence, controlling CO_2 content in gas streams and its emission to the atmosphere is imminent. Practical techniques of capturing CO_2 in the gas/liquid state in direct contact through physical or chemical absorption processes are widespread best exemplified by packed towers, tray towers and bubble columns. However, these methods possess weaknesses such as low contact area, tremendous energy consumption, and may result in operational drawbacks such as weeping, foaming and flooding. The higher efficiency offered by membrane contactors for CO_2 removal and their beneficial advantages in terms of capital investments, operational costs and energy savings due to the miniaturization of the conventional processes has gained attention towards this process [1,2]. Membrane contactors are regarded to be better than conventional dispersed phase contactors because they possess no flooding at high flow rates, no unloading at low flow rates, absence of emulsions, and no requirement for density difference between the two fluids contacted [3]. They reduce the volume of equipment and offer a bigger interfacial area in a non-dispersive contact across a membrane, leading to the decrease of the HTU (height of a transfer unit) values, hence achieving a higher value of the mass transfer coefficient [4]. To fully exploit the growing opportunities in the field of membrane contactor processes, precedence has been given to the identification of new membrane materials that comply with the current requirements. The criteria for selecting membrane materials for a given separation process are complex which include durability, mechanical integrity at operating conditions, high transmembrane flux and hydrophobicity.

The transport of gas in a membrane contactor is based on a diffusion mechanism that allows the gas to flow from one end of the pore in contact with the gas to the gas/liquid interface at the other end of the pore. The separation performance in these processes is determined by the distribution coefficient of a component in two phases and the membrane acts only as an interface. [5]. Therefore, the membrane must possess high hydrophobicity with small pore size to prevent wetting and high permeability to increase diffusion rate [6]. Hence, there is a need to carefully choose the membrane materials to prepare membranes with improved structure to fulfill the requirements of gas/liquid contacting processes. Regardless of the above advantages, a clear drawback of the membrane contactors is the presence of membrane barrier between the two phases separated by the membrane,

which introduces an extra resistance to the overall mass transfer process. Therefore, the membrane applied should possess a high bulk porosity to minimize the fraction of the membrane resistance. Unfortunately, a membrane with high bulk porosity may lead to a membrane with a higher wetting affinity. Therefore, its use is limited due to membrane wetting problems in the operation step, longevity and its high membrane cost. Complete or even partial wetting of the membrane pores by the liquid results in a dramatic decrease in the mass transfer flux due to an excess resistance produced by the stagnant liquid phase trapped inside the pores [7]. Hence, in order to employ an efficient membrane contactor, the membrane wetting phenomena must be prevented [8,9].

Essentially, there are three categories of techniques to overcome membrane wetting, hence improving the process performance, namely by surface modification (to increase the surface hydrophobicity), tuning the membrane structural parameters (pore size distribution and membrane porosity) and the operating conditions. Various physical and chemical techniques were performed for membrane surface modification including coating, grafting, plasma polymerization, etc. **[10].** Among these techniques, surface modification by applying a coating of hydrophobic materials is the main concern in the current work to eliminate membrane wetting in hollow fibers membrane contactors. However, a dense layer of the coating material will introduce an additional resistance to the mass transfer which will inevitably lead to the reduction of the mass transfer rate i.e. the transmembrane flux of the membrane. The reduction of the mass transfer rate due to the membrane resistance has been advised to be compensated by an elevation of the feed gas pressure, i.e., by increasing the driving force **[11]**.

Kreulen et al. **[12]** performed a series of experiments to absorb CO_2 and N_2O via MC. Different polypropylene (PP) hollow fibers including silicon rubber coated hollow fibers were utilized. They concluded that no significant mass transfer reduction occurred after adding a silicone layer. In 1994, Papadopoulos and Sirkar prepared a hollow fiber membrane contactor by using a thin nonporous silicone layer to handle higher gas pressures. It was reported that the aqueous 20% diethanol amine (DEA) led to a substantially higher overall CO_2 permeability and selectivity **[13].** Bessarabov et al. fabricated flat sheet polymeric composite membranes for CO_2 separation to operate as a bubble free process. However, they did not report any comparison between coated and uncoated membrane flat sheets **[14]**. Nymeijer et al. reported the results of PP/ethylene propylene diene terpolymer (EPDM) (1 wt.% in n-hexane) coated hollow fibers for separation of ethane/ethylene mixture. They showed

that the membrane performance remained constant for more than 20 weeks. However, the comparison of the absorption flux of the coated membranes with the neat membranes was not reported [15]. In 2006, Kneifel et al. investigated the performance of polyetherimide hollow fiber membranes coated with a thin dense layer of polydimethylsiloxane (PDMS) with respect to the water vapor permeance to control air humidity. It was shown that the negative effect of the coating on the permeance could be restricted to a permeance loss of about 20% by applying a very thin coating layer [16]. Jin et al. spun hollow fibers from materials made of poly(phthalazinone ether sulfone ketone) (PPESK). The membrane surface was then modified by a coating layer of hydrophobic PDMS and sol–gel polytrifluoropropylsiloxane. The stability of the membranes was evaluated by long-term experiments. Unfortunately, they did not report any comparison between the neat and the coated HF membranes [17]. Nguyen et al. reported a research on fabricating composite membranes for CO_2 separation via monoethanol amine. The composite membrane comprised of polypropylene as the support layer and poly(1-(trimethylsilyl)-1-propyne) (PTMSP) or Teflon AF2400 as the dense top layer. They concluded that a dense skin, when carefully selected and coated, can provide protection from not only the wetting effect to the support but also towards chemical and thermal degradation [18]. A brief review on hollow fiber coating in the application of membrane contactor is shown in Table 1.

As shown in the table, currently none of the works have investigated the effect of silicon rubber coating on a porous support while the resulting pores are still kept open after the coating. Therefore, the scope of this work was coating the surface of the polyetherimide hollow fiber membranes by applying PDMS while keeping the membrane pores open, and investigating the effects of various parameters such as PDMS concentration and procedure of different protocols of coating on the structural parameters of the membranes along with the performance of the gas absorption process.

Table 1. A brief review on the coating of hollow fiber membrane for gas/liquid contactor

2. Theoretical Framework

A vast number of researchers devoted their interests to the partial wetting of hollow fibers in the membrane contactor process [19-22]. Fig. 1 demonstrates the different gas/liquid contact configurations and the concentration gradient of CO_2 in the bulk and boundary layer of gas phase,

the membranes structure and the bulk and boundary layer of liquid phase, including: a) partially wetted porous membrane contactor, b) fully dry porous membrane contactor, c) porous membrane contactor possessing a dense hydrophobic skin layer, and d) porous membrane contactor possessing a porous hydrophobic skin layer. In all the above cases, the gas stream is assumed to be a pure gas, e.g. CO_2. Besides that, in all the cases, CO_2 is finally dissolved in an aqueous solution i.e. water, which is carried out by the solution stream. The controlling parameter is equated to the rate of CO_2 diffusion in the pores. When the pores are gas-filled, CO_2 molecules diffuse in the gas phase, whereas when the pores are partially or totally liquid-filled, CO_2 molecules inevitably diffuse in the liquid phase. Generally, the diffusion coefficients of gas molecules in a gaseous phase relative to a liquid phase is substantially higher by a factor of $10^4 - 10^5$. Therefore the gas absorption flux is controlled by the extent of pore wetting. Case 'a' shows a membrane which is partially wetted. Here, the absorbent solution can penetrate into the membrane gas-filled pores, resulting in a substantial increase of mass transfer resistance against CO_2 pore diffusion. Case 'b' illustrates an ideal membrane which possesses fully liquid-untouched pores. There is no barrier except the gas diffusion through the pores, and hence its absorption performance is the highest among all of the considered cases [19,20]. In case 'c', a nonporous dense hydrophobic coating layer is fully applied onto the skin layer of the support membrane. It was clear that no solution could pass through the coated layer and penetrate into the pores. Hence, we obtain a fully dry system. However, an extra resistance due to the dense coated layer is introduced to the system overall mass transfer resistance. Finally, we have the case 'd' which is the scope of the present work. This case demonstrates a membrane possessing a hydrophobic porous layer coated on top of the support layer. In contrast to case 'c', ideally no extra mass transfer resistance due to the coating layer will be added to the system. Consequently, case'd' includes the hydrophobic character of case 'c' as well, which protects the membrane pores against wetting. This in turn exhibits the gas-filled pore character of case 'b' as well. It is noted that, the thickness of the coating layer is practically negligible with respect to the membrane thickness. However, the coating may lead to change in the surface porosity or mean pore size, which will be discussed in more details shortly.

Considering Fig. 1, the most number of similarities can be found between case 'b', and case 'd'. It is obvious that case 'b' and 'd' display the least membrane mass transfer resistance. This was shown experimentally by Nguyen et al. **[9]**. Nevertheless, in case 'd', depending on the coating procedure, some of the pores might have been partially blocked during the coating step, as a result, the mass

transfer resistance could be slightly to strongly higher than case 'b'. Because of this, in the current work, experiments were conducted in the attempt to materialize this concept.

Fig. 1. a schematic of different concentration gradient of CO_2 in the bulk and boundary layer in gas phase, liquid phase and the membranes structure, *a*) partially wet porous membrane contactor, *b*) fully dry porous membrane contactor, *c*) porous membrane contactor possessing a dense hydrophobic skin layer, *d*) porous membrane contactor possessing a porous hydrophobic skin layer.(GB: gas bulk, GBL: gas boundary layer, LB: liquid bulk, and LBL: liquid boundary layer, and the colors represent the following media; yellow: gas stream, blue: liquid stream, gray: porous membrane cross section and black: coating layer)

3. Experimental

3.1. Raw material

The membranes were prepared from a commercial Ultem® 1000 polyetherimide (PEI) supplied by GE plastic USA. N-methyl-2-pyrrolidone (NMP) used as solvent was supplied by Merck. A rubbery silicone polymer (Sylgard 184) supplied by Dow Corning USA was used as the coating agent. PEI pellets were preconditioned in a vacuum oven at 80 °C for 72 h to remove trapped moisture. All materials were used as received.

3.2. Dope preparation

To prepare casting solution, the polymer was divided into three portions and they were added to the solvent consecutively with a time interval of 15 min. The polymer (12 or 15 wt.%)/solvent mixture was then stirred for 18 h at 60 °C to ensure complete dissolution of the polymer. The solution was further degassed under ultrasonication for 2 h and was left overnight before performing the spinning process.

3.3. Asymmetric polyetherimide hollow fiber membrane preparation

Wet spinning technique, without any air gap, was employed in fabricating asymmetric PEI hollow fiber membrane for this study.

The spinneret used for spinning has a dimension of 1.25 mm for outer diameter (OD) and 0.55 mm for inner diameter (ID). The polymer dope was sent to the spinneret by a constant flow rate of 4.0 cm^3/min at room temperature (~23 ºC) applying a syringe pump to pressurize the polymer dope to pass the spinneret. Another syringe pump was used to deliver the bore fluid (distilled water) by a constant flow rate of 1.7 cm^3/min. Tap water with the temperature of ~23◦C was used for the external coagulant. After completing the spinning, to ensure that all of the solvent in the membrane structure was removed, membranes were immersed in water for 3 days, with daily change of water to remove the residual solvent, followed by drying for 3 to 4 days at room temperature. The OD/ID of the prepared hollow fibers were 0.67/0.41 mm and 0.73/0.44 mm for PEI-12 wt.% and PEI-15 wt.% respectively.

3.4. Membrane coating

The hollow fiber membranes were coated via a rubbery silicone polymer (Dow Corning Sylgard 184). The intention of the coating is to modify the external or the internal surface of the membranes from a hydrophilic surface to an hydrophobic surface. Membranes were submerged into a 0.5% w/w solution of silicone rubber in *n*-hexane for 1 to 2 s under nitrogen blowing conditions through the membranes lumen side. In order to perform the coating onto the inner surface, the silicon rubber solution (0.1%, 0.2% and 0.5% w/w solution) was fed into the lumen of the fibers, then the solution was discharged by applying a nitrogen gas stream. The thickness of the silicone layer was varied as a function of the concentration of the coating solution. The coated membranes were subsequently placed in an oven at ~60 °C for 24 hours to ensure curing the coating layer before performing the gas permeation testing (GPT) and contactor performance testing. The code and specifications of the fabricated membranes are summarized in Table 2.

Table 2. Code and specifications of the fabricated membranes before and after coating

3.5. Gas permeation test

Two to three hollow fibres were glued with epoxy resin at one end and the other end was potted to a stainless steel fitting inserted into a stainless steel cylinder. The GPT system is shown schematically in Fig. 2. The feed gas (He 99.97 vol.%) was supplied to the lumen side of the membranes and the pressure was controlled by a pressure regulator. The rate of gas permeation was measured using a constant-pressure method. For measuring the permeation rate a soap bubble flow meter was utilized. The permeation tests were carried out at 23 °C and feed side pressure was varied from 25 kPa to 350 kPa gage depend on the permeation rate of the membranes. Permeance was calculated as follows:

$$\mathrm{P} = \frac{101325}{RTA\Delta p}\frac{\Delta V}{\Delta t} \qquad (1)$$

where P is the gas permeance (mol m^{-2} Pa^{-1} s^{-1}), R is the universal gas constant (8.314 J mol^{-1} K^{-1}), T is the system absolute temperature (K), V is the volume of gas permeated through the membrane (m^3, STP), A is the effective membrane area (m^2), t is the permeation time (s) and Δp is the transmembrane pressure drop (Pa). It is noted that, the constant 101325 is the absolute atmospheric pressure of the permeate side in Pa.

Fig. 2. Gas permeation testing rig

3.6. Measurement of Critical entry pressure of water and Contact angle

Critical entry pressure of water (CEPw) test is to measure the minimum pressure required to let water penetrate through the membrane pores and is used as an indication of wettability resistance of the membrane. Distilled water was pressurised into the lumen side of the dried hollow fibre membrane and the pressure was increased gradually at a step size of 50 kPa gauge. The pressure at which the first droplet of water appears on the outer surface of the membrane was recorded as CEPw, which is the minimum pressure required to drive water through the largest membrane pores.

Water contact angle measurement is a simple way to quantify the hydrophilicity/hydrophobicity characteristic of the membranes surface. The contact angle of the outer and inner surface of the membranes was measured by a contact angle meter (model OCA20, Dataphysics, Germany) and distilled water was used as the probe liquid. The contact angle was recorded immediately after putting a tiny droplet of water on the membranes. At least 10 points were used for the contact angle measurement and the average values were reported.

3.7. Gas absorption test

To evaluate the performance of silicon rubber coated membranes, the fibres were assembled in a membrane contactor module and CO_2 absorption tests were conducted. The following two cases were considered: running pure CO_2 in the shell side and distilled water in the lumen side and conversely, pure CO_2 in the lumen side and distilled water in the shell side. Eight PEI hollow fibre membranes were assembled in a contactor module with inner diameter of 1.57 cm. The effective length of the fibres in the module was 18 cm. The membrane gas absorption rig is shown schematically in Fig. 3. A diaphragm pump was used to flow distilled water at a constant pressure. The liquid pressure was adjusted so that it was 50 kPa higher than the pressure of the CO_2 gas to prevent undesired bubbling. Through all of the experiments, the gas flow rate was set constant at 1.0 dm^3/min. The collected sample of the absorbed CO_2 into water was immediately titrated by a solution of 0.05 M NaOH, where Phenolphthalein was applied as the equivalent point indicator **[23]**.

Referring to appendix A, the concentration of $[H^+]$ can be evaluated and finally calculate the pH of the system. Accordingly, the maximum CO_2 captured by pure water at atmospheric pressure and room temperature provides a pH of almost 5.65. It is noted, the measured pH occurred between ~5.5 and ~6.8 as was reported by the others [24].

Fig. 3. Gas absorption rig (Orange: CO_2, blue: distilled water and green: CO_2 solution).

The experimental flux can be calculated by a simple mass balance of CO_2 over the entire effective length of the membrane module:

$$J = \frac{Q_L(C_L^{out} - C_L^{in})}{n\pi dL} \quad (2)$$

where Q_L is the liquid volumetric flow rate (m^3/s), J is the gas absorption flux (mol m^{-2} s^{-1}), C_L^{out} and C_L^{in} are the concentration of CO_2 in the outlet and inlet solution (mol/m^3) respectively, depending on lumen or shell side liquid flow, d is inside or outside fiber diameter (m), n number of hollow fibers and L is the length of the fibers (m). Also the theoretical flux can be obtained by:

$$J = K_{OL}(\Delta C_{lm}) \quad (3)$$

where K_{OL} is the overall mass transfer coefficient (m/s) based on the liquid phase and (ΔC_{lm}) is a log-mean concentration difference of CO_2 between the input and output of the CO_2 solution. Equating Eq. (2) and (3), one can calculate the overall mass transfer coefficient [25]:

$$K_{OL} = \frac{Q_L(C_L^{out} - C_L^{in})}{n\pi dL(\Delta C_{lm})} \quad (4)$$

and (ΔC_{lm}) is defined as [25]:

$$(\Delta C_{lm}) = \frac{(C_L^{out,i} - C_L^{out}) - (C_L^{in,i} - C_L^{in})}{\ln\left(\frac{C_L^{out,i} - C_L^{out}}{C_L^{in,i} - C_L^{in}}\right)} \quad (5)$$

where $C_L^{out,i}$, $C_L^{in,i}$ are the concentration of CO_2 in liquid which is in equilibrium with pure CO_2 at the liquid/gas interface in the outlet and inlet solution (mol/m^3) respectively. Considering establishment of the equilibrium condition, the concentration of CO_2 at the liquid/gas interface can be estimated by Henry's law given by Eq. (6):

$$C_L^i = HC_G^i \quad (6)$$

where C^i_G is the concentration of CO_2 at the liquid/gas interface for gas phase (mol/m^3) and H is a dimensionless temperature-dependent Henry constant which is obtained by Eq. (7) [26].

$$H = \frac{0.461884T}{h} \quad (7)$$

and h is a Henry constant with dimension of pressure (MPa) for CO_2 dissolved in water as well computed by [26]:

$$\ln(h) = -6.8346 + \frac{1.2817\times10^4}{T} - \frac{3.7668\times10^6}{T^2} + \frac{2.9970\times10^8}{T^3} \quad (8)$$

It is noted that since the gas phase is pure CO_2, as a result, in the gas phase the interface concentration of CO_2 is equal to the bulk concentration of CO_2.

3.8. Overall and membrane mass transfer coefficient, resistance-in-series model

The mass transfer coefficient of the liquid boundary layer for the lumen side is mainly determined by the system geometry and flow condition, for which many correlations are available to predict it [27,28]. An approximate solution for the differential equation driven from the continuity equation was proposed by Graetz. For more details please refer to appendix B [**29**]. In membrane contactor systems, the Wilson plot is widely applied to determine the membrane mass transfer. The mass transfer resistance of the liquid side is proportional to the liquid velocity as $v^{-\alpha}$, where α is an empirical parameter and v is the liquid velocity. A plot of $1/K_{OL}$ versus $v^{-\alpha}$ results in a straight line, which is known as Wilson plot. Then the membrane mass transfer resistance can be calculated from the intercept of the plot. It is believed that this method is more accurate than the predictions achieved by the traditional correlations for Sherwood number, therefore this method was applied throughout the current study.

According to the resistance-in-series model (Eq. 9), the overall mass transfer resistance consists of three major resistances: gas boundary layer, liquid boundary layer and membrane mass transfer resistances.

$$\frac{1}{K_{OL}} = \frac{1}{k_L} + \frac{Hd_i}{k_M d_{lm}} + \frac{d_i}{k_G d_o} \quad (9)$$

where K_{OL}, k_L, k_G and k_M are overall liquid, liquid boundary layer, gas boundary layer and membrane mass transfer coefficient (m/s) and d_i, d_o and d_{lm} are hollow fiber inside, outside and log mean diameters (m). In particular, the membrane mass transfer resistance can be written as

$$R_M = \frac{Hd_i}{k_M d_{lm}} \tag{10}$$

(It should be noted that Eqs. (9) and (10) are given for the case when the liquid flows in the lumen. When the liquid flows on the shell side subscript i and o should be exchanged.)

When the gas side is a single component, which here is the present case, the resistance in the gas boundary layer can be neglected.

On the other hand, assuming the membrane pores are gas filled and the mass transfer in the pore is entirely by diffusion without convection, membrane mass transfer coefficient is given by,

$$\frac{1}{k_M} = \frac{\tau}{D_G}\frac{l_p}{\varepsilon} \tag{11}$$

where τ is the tortuosity of the skin layer which can be roughly considered as unity due to the tiny thickness of the skin layer. D_G (m^2/s) is the diffusion coefficient of gas. Further assuming that the diffusion is primarily contributed by Knudsen and molecular diffusion, D_G is given by [33]:

$$\frac{1}{D_G} = \frac{1}{D_K} + \frac{1}{D_M} \tag{12}$$

For more information on how to estimate the Knudsen and molecular diffusion coefficients the readers can refer to appendix B.

3.9. Scanning electron microscopy (SEM)

Scanning electron microscope (SEM, Hitachi, TM-3000) was used to study the morphology of the membranes produced. The hollow fibers were broken in liquid nitrogen carefully to make smooth surface. The fractured fibers were placed on a disc for sputtering with a thin film of platinum. Then,

they were mounted on a stainless steel stand with carbon tape. The SEM micrographs of cross-section of the hollow fibers were taken at various magnifications.

4. Results and Discussion

4.1.Gas permeation results

Fig. 4 illustrates the helium permeance of neat and inside coated hollow fiber membranes. According to the figure, silicon rubber coating reduced the permeance of helium gas. Nonetheless, among the PDMS coated membranes, as the silicone rubber concentration increased, the permeance increased as well. Thus, membrane M-12-0.1-IC had the lowest gas permeance while membrane M-12-0.5-IC displayed the highest.

Fig. 4. Helium permeance of neat and inside silicon rubber coated PEI-12wt.% hollow fiber membranes

Fig. 5 shows the permeance of helium for neat and outside coated hollow fiber membranes. The permeance decreased dramatically by an order of magnitude when silicone rubber coating was applied without N_2 blowing. When N_2 gas was blown from the lumen side, the permeance increased dramatically and even surpassed that of the neat hollow fiber. The decrease in the permeance was most probably due to the blockage of the small pores, which resulted in shifting the mean pore size towards larger and a sharp decrease in the effective porosity. On the other hand, when the N_2 gas pressure was applied on the lumen side, the pores were kept open during the coating process, maintaining or even enlarging the pore size and porosity caused by stretching a result of the gas pressure. Consequently, an increase in the gas permeance as well as enhancement in the gas absorption flux was expected. Interestingly, membrane M-15-0.5-IC demonstrated the same behavior as membrane M-15-0.5-WB. According to this observation, it was concluded that the effect of inside and outside coating is meaningfully the same which seems to be reasonable.

Fig. 5. Helium permeance of neat and silicon rubber coated PEI-15wt.% hollow fiber membranes

Table 3 summarizes the structural parameters of silicon rubber coated hollow fiber membranes in comparison to the uncoated one. In the current study, the data obtained by the partial slip model (Appendix C), which might be more reliable than the conventional GPT model, were used for further discussions. Looking into the data of M-12, M-12-0.1-IC, M-12-0.2-IC and M-12-0.5-IC hollow

fibers, r_p increased from M-12 to M-12-0.1-IC and then kept decreasing from M-12-0.1-IC to M-12-0.5-IC with an increase in silicon rubber concentration in the coating solution. On the other hand, ε/l_p, showed an opposite trend.

These observed trends was explained by assuming penetration of low viscosity and low surface tension silicon rubber solution (0.1 %) deep into a large number of small pores and consequent significant pore blocking. On the other hand, penetration of high viscosity and high surface tension silicon rubber solution (0.5%) was allowed only to enter the larger pores with less severe pore blocking. The mode of pore blocking is schematically illustrated in Fig. 6 for: a) uncoated membranes, b) coated membranes via a coating solution of low silicon rubber concentration, and c) coated membranes via a high silicon rubber concentration. These observations showed a significant influence of the silicon rubber layer even at very low concentration, which shows the role of this key-parameter in controlling the final performance properties of the membranes.

Table 3. Prediction of pore size and effective surface porosity by Partial slip model (ψ=0.5), using helium as probe gas at room temperature.

Fig. 6. Tiny and large pores in the inner skin layer of the coated and uncoated membranes at different concentration of silicon rubber solution, a) uncoated, b) 0.1 wt.% or 0.2 wt.% and, c)0.5 wt.%.(Black: Silicon rubber, Gray: Membrane matrix, White: pore channels)

4.2.Morphological study

Fig. 7 depicts the SEM spectra of the cross-section and the inner surface of the coated hollow fiber membranes. The SEM images were similar for all PEI coated hollow fibers. The cross-section of the PEI membranes mostly shows a thick layer of fingerlike structure, which starts from both the outer and inner skins and meet with each other at the midway. According to the SEM images, since low concentrations of silicon rubber solution i.e. 0.1%, 0.2% and 0.5% w/w, were applied, the thickness of the silicon rubber layer is very tiny and is not clearly observable, it is noted that applying a more powerful machine e.g. field emission scanning microscopy (FESEM) probably the thickness of the coating layer could be seen.

Fig. 7. SEM spectra of the cross-section and the inner coated surface of a) M-12-0.1-IC, b) M-12-0.2-IC, c) M-12-0.5-IC. The magnification of the top right small spectrum, from the left are X600, X600 and X800 respectively and the scale bar is 100 μm.

4.3. Wettability Resistance

Table 4 shows the influence of different coating protocols on the contact angle and CEPw of the membranes. From Table 4, M-15 and M-12 membranes displayed contact angle of 82° and 77°, respectively. The silicon rubber coated membranes, on the other hand, exhibited much higher contact angles of above 108°. These results indicated that while the silicon rubber coating layer remained porous, even a thin layer of the coated PDMS (Fig. 7) could increase the contact angle significantly. Moreover, a very thin coated layer could substantially affect the hydrophobicity property of the membranes and improve the wettability resistance by a large extent.

Table 4 also includes the CEPw data of the coated and uncoated membranes. The CEPws for the uncoated membranes M-15 and M-12 were 800 and 300 kPa, respectively. Looking at the data for M-12-IC (inside coating) series, an increase in silicon rubber concentration would result in an increased CEPw, eventually reaching 600 kPa for M-12-0.5-IC, which was a 100 % increase relative to M-12. It is likely that an increase in silicon concentration would result in an increase in the thickness of the silicon rubber layer, which in turn led to the increase of the membrane CEPw. This was optimal with the contact angle of 114° for M-15-0.5-IC. According to Table 3, membrane M-12-0.1-IC had the highest mean pore size and the lowest surface porosity. As a result, the lowest gas permeance observed was due to the lowest surface porosity and the lowest CEPw measured was due to the highest mean pore size. Moreover, based on our observations, applying different concentration of silicon rubber coating solution had two modes of action. First, increasing the concentration led to the decrease in mean pore size and increase in surface porosity. Second, increasing the concentration resulted in the shifting of the surface property from hydrophilic to hydrophobic. Therefore, an increase in the silicon rubber solution caused an increase in the membrane CEPw. Since water was supplied into the lumen side of the hollow fiber, the effect of outside coating was much less

pronounced. Based on the above observations, the coating technique showed significant dramatic changes in both contact angle and CEPw for both the inside and outside coated hollow fiber membranes.

Table 4. Contact angle and CEPw of the coated and uncoated hollow fiber membranes.

4.4.Membrane mass transfer resistance

In order to better understand the membrane mass transfer resistances (R_M), the Wilson plot of $1/K_{OL}$ versus $v^{-\alpha}$ was used, Fig. 8. K_{OL} was obtained from the experiments using Eq. (4). As a result, the R_M was obtained from the intercept of the Wilson plot. Among various $1/K_{OL}$ versus $v^{-\alpha}$ correlation, the α value of almost 0.47 represented the best linear fit to the data points. The linear trend lines fitted through the experimental points are shown in Fig. 8 as well. It is noted that in the original Wilson plot, the predictions was based on an α value of 0.33 [**33**]. Atchariyawut et al [36] and Ismail and Mansourizadeh [23] reported α values of 0.93 and 0.53 respectively for PVDF hollow fiber membranes. According to Fig. 8, the overall mass transfer resistance decreases as the concentration of PDMS solution increases. Comparing the overall mass transfer resistance of the membranes, membrane M-12-0.5-IC exhibited the lowest resistance among the coated membranes. This was consistent with the gas permeation results in Fig. 4. Interestingly, the pore size and the effective porosity of this membrane were the largest and the contact angle was the highest (see Table 3 and 4). This means that this membrane was the most efficient among all the other tested membranes.

Fig. 8. Wilson plot of the fabricated membranes, effect of silicon rubber lumen side coating on the MCs overall mass transfer resistances ($\alpha \approx 0.47$)

The liquid mass transfer resistances associated with the uncoated and coated membranes can be estimated by the aid of resistance-in-series model as well. The method of obtaining the individual resistances is as follows. Ignoring the contribution of gas phase resistance, applying resistance-in-series model i.e. Eq. (9):

$$R_{OL} = R_L + R_M \qquad (13)$$

Where R_{OL} and R_L are defined as $1/K_{OL}$ and $1/k_L$, respectively. K_{OL} (and R_{OL}) is obtained from the experiments using Eq. (4). R_M was already obtained from the intercept of the Wilson plot in Fig. 8. Hence, by subtracting R_M from R_{OL}, one can obtain the R_L at each desirable flow rate. The results for a liquid velocity of 3.0 m/s are typically shown in Table 5.

The membrane mass transfer coefficient as well as the membrane mass transfer resistance can be estimated by applying the GPT results along with Equations (10) to (12) and Equations (B5) to (B8). An acceptable agreement between the gas absorption approach and gas permeation approach can be achieved while the pores are fully filled with gas . Table 5 illustrates a good agreement between the two approaches except for membrane M-12. The difference was most likely attributed to the partial pore wetting of membrane M-12, which resulted in higher membrane mass transfer resistance during the gas absorption process. By comparing the membrane mass transfer resistances estimated by the two approaches depicted in Table 5, this phenomenon is revealed. It is noted that R_L contributes to R_{OL} more effectively than R_m. In addition, R_L does not substantially depend on the membrane, which seems to be reasonable because the fluid dynamics of the liquid phase on the lumen side is almost the same for all hollow fibers. The authors believe that this was due to the liquid boundary layer resistance which was stronger than the membrane resistance. Moreover, the liquid phase mass transfer coefficient was a strong function of turbulence, and in this case, the liquid boundary resistance was almost constant for all hollow fibers since it was kept constant at liquid velocity of 3.0 m/s. On the other hand, since increasing the coating solution concentration would the effective porosity of the PDMS coated membranes, the membrane mass transfer resistance experienced a decrease as well. Results depicted in Tables 3, 4 and 5 disclosed that the final performance of the PDMS coated membranes was resulted from the simultaneous effect of the increase in the hydrophobicity character of the membranes combined with the decrease in the effective porosity of the membranes.

Table 5. Comparison between membrane mass transfer resistances based on gas absorption results and gas permeation results.

4.5.Membrane contactor performance

Fig. 9 depicts CO_2 absorption flux vs. water velocity of the outside coated membranes in comparison to the uncoated one. CO_2 absorption flux depends on the type of the absorbent utilized, the system pressure and temperature, the membrane hydrophobicity (which control the degree of partial wetting of the pores) and the membrane structural parameters (mean pore size and the effective porosity). From Fig. 9 it can be observed that the CO_2 flux of membrane M-15-0.5-WB is lower than M-15. This was likely attributed to the blockage of the pore mouth at the outside surface of the hollow fibers by a silicon rubber layer, which results in the increase in the pore size, as well as a decrease in the effective porosity (see Table 3 and Fig. 6b). This is also in good agreement with the GPT results as shown in Fig. 5 and Table 3. Conversely, the flux of M-15-0.5-600B was higher than that of M-15 due to the increase in both pore size and effective porosity (see Table 3). The surface contact angle also increased significantly from M-15 to M-15-0.5-600B (see Table 4). Probably, the increase in surface hydrophobicity was prevented by the partial pore wetting which led to a significant increase in membrane resistance against pore wetting.

Fig. 9. CO_2 absorption flux vs. liquid velocity through shell side, effect of nitrogen blowing during the silicon rubber coating onto outside surface of the 15% PEI hollow fiber membranes on the MCs performance.

Fig. 10 shows the performance of the uncoated membranes M-15 and M-12, in comparison to the silicon rubber coated membranes M-15-0.5-IC and M-12-0.5-IC.

Fig. 10. CO_2 absorption flux vs. liquid velocity through lumen, effect of silicon rubber lumen side coating on the MCs performance for 15% PEI and 12%PEI hollow fibers.

The flux of both M-12 and M-15 hollow fibers was decreased slightly by silicon rubber coating. However, the flux of M-12-0.5-IC hollow fiber was several times higher than M-15-0.5-IC even after the silicon rubber coating. The trend of the absorption flux is in close agreement with the structural parameters shown in Table 5. Fig. 11 shows the effect of inside silicone rubber coating on the hollow fiber performance. Fig. 11 exhibits the effect of different concentration of silicon rubber solution on the performance of the PDMS coated 12 wt.% PEI membranes. The trend in the flux change observed in Fig. 11 parallels the change in R_{OL}, which seems to be reasonable. The CO_2 absorption flux of M-12-0.5-IC is the highest among the all coated membranes. Interestingly, M-12-0.2-IC and M-12-0.1-IC showed the same degree of performance in terms of CO_2 absorption flux, which is lower than untreated membrane and membrane M-12-0.5-IC. Most likely, the very low

concentration of silicon rubber solution of 0.1 and 0.2 wt.%, penetrated through the pores of the membrane inner skin layer, blocking of some of them as well as decreasing the pores sizes of others by coating the pores wall. This explanation is shown schematically in Fig. 6. This phenomenon can be true for membrane M-12-0.5-IC in a lower extent. Generally speaking, the decrease in CO_2 absorption flux is outweighed by the substantial enhancement in the membrane wetting resistant due to the higher contact angle and CEPw of the PDMS coated membranes. Fig. 10 also shows the comparison between the performance of the PVDF membranes fabricated by Mansourizadeh et al. [37] and the fabricated membranes in the current work. The membranes fabricated by Mansourizadeh et al. showed a contact angle of 86° whereas the contact angles of the PDMS coated membrane s are as high as 108°-116°, as shown in Table 4. Moreover, they reported a membrane mass transfer resistance of as high as 37887 s/m, significantly higher than the data presented in Table 5 presented in this work. Because of this, referring to Fig. 10, the performance of the membranes fabricated in the present study shows substantially (one order of magnitude) higher CO_2 absorption flux in comparison to their membranes.

Fig. 11. CO_2 absorption flux vs. liquid velocity through lumen, effect of silicon rubber concentration on the MCs performance for 12 wt% PEI hollow fibers.

The comparison of Fig. 4 and Fig. 5 with Fig. 11 and Fig. 9 respectively shows that the effect of silicon rubber coating on CO_2 absorption flux is less crucial than that of on helium gas permeance. This is most likely postulated to the basic difference in gas diffusion mechanisms between gas permeance and gas absorption flux. In the former, the transmembrane pressure difference is high e.g. up to 500 kPa so that the Knudsen and viscous diffusion are simultaneously controlling the gas permeation process. Meanwhile, in the latter, the value of the transmembrane pressure difference is much lower e.g. less than 50 kPa and the Knudsen and molecular diffusion are controlling the absorption flux. On the other hand, CO_2 permeability is much higher than helium gas through silicon rubber (2700/300, nine times) [38], therefore the closed pores combined with the open pores participate in the mass transfer process to deliver a portion of CO_2 to the other side of the membranes to enhance the gas absorption flux. Table 6 explains this fact in a more quantitative manner. Table 6 illustrates the ratio of $(\varepsilon/lp)/(\varepsilon/lp)_{M\text{-}12}$, $P/P_{M\text{-}12}$ calculated from the GPT results shown in Table 3 and $J/J_{M\text{-}12}$ related to the gas absorption flux extracted from Fig. 11. The parameters without subscription belong to the coated membranes. From Table 6, the trend of the

ratios of the gas permeances (P/P_{M-12}) are almost proportional to the ratios of the effective porosities ($(\varepsilon/lp)/(\varepsilon/lp)_{M-12}$), whilst the ratio of the gas absorption fluxes (J/J_{M-12}) are substantially higher as well as more constant with respect to the ratio of gas permeation results, i.e. the effective porosities and the gas permeances.

Table 6. The effect of silicon rubber coating on the helium GPT results and carbon dioxide absorption flux.

5. Conclusion

Based on the observations, the coating technique showed a significant change in the contact angle and CEPw of the coated membranes for the inside and outside coated hollow fiber membranes in common, while the silicon rubber coating layer remained porous. Disregarding the method of coating and even the polymer concentration, the contact angle was enhanced drastically from 82° (or 78°) up to at least 111° (or 108°). The CO_2 absorption results revealed that by blowing nitrogen (600 kPa) through the lumen side of the hollow fibers during the PDMS coating process onto the membranes outside surface, the absorption flux of the membranes increased. A little decrease in CO2 absorption flux for the other cases was outweighed by substantial enhancement in the membrane wetting resistance due to the high contact angle and CEPw. It is believed that this was due to prohibiting the membrane pores from partial pore wetting, which is a huge barrier across the mass transfer through the membranes. Based on this study, the increment in the ratio of the gas permeances were proportional to the ratio of the effective porosities, whilst the ratio of the gas absorption fluxes were substantially higher as well as more constant than the gas permeation results. This is most likely due to the involvement of the combination of closed pores and open pores in the mass transfer process to deliver CO_2 to the other side of the membranes. This observation showed the high influence of the silicon rubber layer even at very low concentration of silicon rubber solution on the CO_2 gas absorption, which emphasizes the role of this key-parameter in controlling the final membrane contactor performance.

Appendix A: *CO_2 dissolution and dissociation in pure water*

During the absorption process via pure water, the dissolved CO_2 ($CO_{2\,(W)}$) and the undissolved CO_2 ($CO_{2(g)}$) are in equilibrium and are related to each other by the Henry's law:

$CO_{2(g)} \leftrightarrow CO_{2(l)}$ (A1)

Where K_H=29.76 atm/(mol/dm^3) is the henry constant of CO_2 at atmospheric pressure and room temperature [26]. At equilibrium, only a small fraction (ca. 0.2 - 1%) of the dissolved CO_2 which is shown here by ($CO_{2(l)}$) is actually converted to H_2CO_3:

$CO_{2(l)}+H_2O \leftrightarrow H_2CO_{3(aq)}$ (A2)

The hydration equilibrium constant of CO_2 at room temperature [$H_2CO_{3(aq)}$]/[$CO_{2(l)}$] is almost $1.7\times10^{-}$**5** [39], which reveals that the majority of the CO_2 is not converted into carbonic acid, i.e. remaining in the molecular form $CO_{2(molecular)}$. As a result, $CO_{2(l)}$=$CO2_{(molecular)}$+ $H_2CO_{3(aq)}$. Carbonic acid acts as a diprotic acid. Obviously, there are two dissociation constants corresponding to the number of valences. The first constant is responsible for the dissociation into the bicarbonate ion, HCO_3^-:

$H_2CO_{3(aq)} \leftrightarrow HCO_3^- + H^+$ (A3)

Whose dissociation constant is equal to 2.5×10^{-4} **[38].** While applying the first dissociation constant, as mentioned above, CO_2 dissolved in the molecular form ($CO_{2(molecular)}$) is in equilibrium with the dissociable form as carbonic acid ($H_2CO_{3(aq)}$) in the aqueous form. Consequently, H_2CO_3 (with no subscription) combines the dissolved CO_2 both the molecular form and the dissociable forms. Therefore, to cover the two forms of CO_2 presented in pure water, Eq. (A3) can be rearranged as follows:

$H_2CO_3 \leftrightarrow HCO_3^- + H^+$ (A4)

Whose apparent dissociation constant is equal to 4.45×10^{-7} [40].

The second dissociation constant is responsible for the production of carbonate ion, CO_3^{2-}:

$HCO_3^- \leftrightarrow CO_3^{2-} + H^+$ (A5)

Whose dissociation constant is equal to 4.70×10^{-11} [40].

Applying Eqs (A1) and (A3) to (A5), along with the dissociation equation of water $[H^+][OH^-]=10^{-14}$ and the system overall charge balance equation $[H^+]=[OH^-]+[HCO_3^-]+2[CO_3^{2-}]$ the system of equations is closed.

Appendix B: ***Predicting the mass transfer and diffusion coefficients***

An approximate solution for the differential equation driven from the continuity equation was proposed by Graetz for small values of Graetz number, Gz (d^2v/LD_L), by which the average and the local Sherwood number, Sh (k_L/d_hD), can be obtained as follows [29]:

$$Sh = 3.67, \quad Gz < 10 \qquad \text{(B1)}$$

where v is liquid velocity in lumen (m/s), D_L (m^2/s) is the diffusion coefficient of CO_2 in liquid phase, k_L is liquid boundary layer mass transfer coefficient (m/s) and d_h is the hydraulic diameter (m).

Another solution was given by the Leveque equation [29]. The approximate solution proposed by Leveque to the system is based on the assumption that the concentration boundary layer is limited to a thin layer adjacent to the wall of the fiber. This assumption is valid for high mass velocities through relatively short fibers in laminar flow [30]. Therefore, the Leveque equation is mostly applicable for Gz exceeding 20. According to Leveque, Sh is given by:

$$Sh = 1.62Gz^{1/3}, \quad Gz > 20 \qquad \text{(B2)}$$

Many researchers have experienced that for the flow of aqueous solutions at atmospheric pressures, a combination of Graetz and Leveque solution can be effective to predict the lumen-side mass transfer coefficient for gas filled pores. Kreulen et al. [31] gave the generalized solution of Graetz–Leveque equation by curve fitting of Eqs. (B1) and (B2) against experimental data:

$$Sh = \sqrt[3]{3.67^3 + 1.62^3 Gz}, \quad 20 > Gz > 10 \qquad \text{(B3)}$$

In contrast, for the shell side mass transfer coefficient, no common model is available to describe the mass transfer coefficient, most likely because of ununiformed distribution of liquid flow, presence of dead zones, channeling, splitting etc. [27]. These are vastly due to uneven fiber distribution inside the membrane module. One of the most commonly used models is the model proposed by Yang and Cussler [32]:

$$Sh = 1.25(\mathrm{Re} d_{sh}/L)^{0.93} Sc^{0.33} \quad \text{(B4)}$$

Where Re ($\rho_L v d_h/\mu$) is the shell side Reynols number, and Sc ($\mu/\rho_L D_L$) is the liquid Schmidt number. ρ_L is liquid density (kg/m^3), and μ is liquid viscosity (Pa.s).

Molecular diffusion coefficient (D_M) can be easily calculated by Chapman and Cowling [33] equation:

$$D_M = \frac{3}{8}\frac{1}{\sigma^2 n}\sqrt{\frac{1000RT}{\pi M}} \quad \text{(B5)}$$

with

$$n = \frac{6.02\times10^{26}\rho_g}{M} \quad \text{(B6)}$$

and

$$\rho_g = \frac{pM}{1000ZRT} \quad \text{(B7)}$$

where σ is the molecular size which is equal to 3.3×10^{-10} m for CO_2, n is the number density (1/m^3), P is the average pressure between upstream and downstream (Pa), ρ_g is the gas density (kg/m^3), Z is the z-factor which approaches unity for an ideal gas, and R is a universal gas constant (8.314 Pa m^3/mol K).

The Knudsen diffusion coefficient (D_K) is calculated by [33]:

$$D_K = \frac{2}{3} r_p \sqrt{\frac{8000RT}{\pi M}} \quad \text{(B8)}$$

Appendix C: ***Pore size and Effective porosity***

The results of the GPT were used to calculate the pore size and effective porosity. In GPT, it was assumed that the pores are cylindrical and straight and gas flows through the pores. The partial slip model [41, 42] was applied to determine the mean pore size and effective porosity. This model demonstrates the nonlinear trend of the data specially in the range of transition flow between free molecular regime and viscous flow regime. The required equations are as follows:

$$\mathrm{P} = \frac{1}{RT}\left\{\phi \frac{2r_p}{3}\left(\frac{8000RT}{\pi M}\right)^{0.5} + (1-\phi)\left[\psi r_p \left(\frac{1000\pi RT}{8M}\right)^{0.5} + \frac{r_p^2 p}{8\mu}\right]\right\}\frac{\varepsilon}{l_p} \quad \text{(C1)}$$

$$\phi = \frac{1}{1+\frac{1}{k_n}} \quad \text{(C2)}$$

and

$$k_n = \frac{\lambda}{2r_p} \quad \text{(C3)}$$

Where ε is the membrane surface porosity, l_p is the pore length (m) and the ratio ε/l_p is called effective porosity. M is the molecular weight (kg/kmol) and μ is the gas viscosity (Pa.s). ϕ is called wall-molecule collision probability function which shows the nonlinearity of the gas permeance versus average pressure, due to the pressure dependency of slope, and ψ is a factor which shows the extent of the slip flow regime, supposed to be $0.0 < \psi < 1.0$. Here, ψ has been assumed to be 0.5. K_n is the Knudsen number and λ is gas mean free path (m) given by kinetic theory of gases:

$$\lambda = \frac{1}{\sqrt{2}} \frac{k_B T}{\pi \sigma^2 p} \quad \text{(C4)}$$

Where k_B is the Boltzmann constant (equal to 1.38×10^{-23} J/K), σ is the collision diameter (m) and P is system mean pressure (Pa) [43]. The details of derivation of these equations and the simple algorithm utilized to solve r_p and ε/l_p were presented elsewhere [41].

Nomenclature

A	is the effective membrane area (m^2)
C^i_G	concentration of CO_2 at the liquid/gas interface for gas phase (mol/m^3)
C_L^{in}	inlet concentration of CO_2 in solution (mol/m^3)
$C_L^{in,i}$	inlet concentration of CO_2 in liquid/gas interface (mol/m^3)
C_L^{out}	outlet concentration of CO_2 in solution (mol/m^3)
$C_L^{out,i}$	outlet concentration of CO_2 in liquid/gas interface (mol/m^3)
(ΔC_{lm})	log-mean concentration difference
d	inside or outside fiber diameter (m)
d_h	hydraulic diameter (m)
d_i, d_o *and* d_{lm}	hollow fiber inside, outside and log mean diameters (m)
D_G	diffusion coefficient of gas (m^2/s)
D_K	Knudsen diffusion coefficient (m^2/s)
D_L	diffusion coefficient of CO_2 in liquid phase (m^2/s)
D_M	molecular diffusion (m^2/s)
Gz	Graetz number
H	dimensionless temperature-dependent Henry constant
h	Henry constant (MPa)
I	intercept

J	total absorption flux (mol/m^{2}s)
k_B	Boltzmann constant (equal to 1.38×10^{-23} J/K)
k_G	gas boundary layer mass transfer coefficient (m/s)
k_L	liquid boundary layer mass transfer coefficient (m/s)
k_M	membrane mass transfer coefficient (m/s)
K_n	Knudsen number
K_{OL}	overall mass transfer coefficient based on the liquid phase (m/s)
L	length of the fibers (m)
l_p	pore length (m)
M	molecular weight (kg/kmol)
n	number of hollow fibers, gas number density (1/m^3)
P	total permance (mol/m^{2}Pas)
P	system mean pressure (Pa)
ΔP	is the transmembrane pressure drop
Q_L	is the liquid volumetric flow rate (m^3/s),
R	is the universal gas constant (8.314 J mol^{-1} K^{-1})
Re	shell side Reynols number
R_L	liquid boundary layer mass transfer resistance (s/m)
R_M	membrane mass transfer resistance (s/m)
R_{OL}	overall membrane mass transfer resistance (s/m)
r_p	pore radius
S	slope
Sc	liquid Schmidt number.
Sh	Sherwood number
t	is the permeation time (s)
T	system absolute temperature (K
V	is the volume of gas permeated through the membrane (m^3, STP)
Z	z-factor
ε	membrane surface porosity
ε/l_p	effective porosity
ϕ	wall-molecule collision probability function

λ	gas mean free path (m)
μ	gas viscosity (Pa.s).
ρ_L	liquid density (kg/m3)
ρ_G	gas density (kg/m3)
σ	collision diameter (m)
σ	molecular size(m)
τ	tortuosity
v	is liquid velocity in lumen (m/s),
ψ	slip flow regime factor

References

[1] D. deMontigny, P. Tontiwachwuthikul, A. Chakma, Comparing the absorption performance of packed columns and membrane contactors, Ind. Eng. Chem. Res. 2005, vol. 44, pp. 5726–5732.

[2] S. Mosadegh-Sedghi, D. Rodrigue, J. Brisson, and M. C. Iliuta, Wetting phenomenon in membrane contactors – Causes and prevention, J. Membr. Sci. 2014, vol. 452, pp. 332–353.

[3] S. Khaisri, D. deMontigny, P. Tontiwachwuthikul, and R. Jiraratananon, A mathematical model for gas absorption membrane contactors that studies , the effect of partially wetted membranes, J. Membr. Sci. 2010, vol. 347, pp. 228–239.

[4] M. Stanojevic, B. Lazarevic, and D. Radic, Review of membrane contactors designs and applications of different modules in industry, FME Transactions, 2003, vol. 31, pp. 91-98.

[5] M. Mulder, Basic Principles of Membrane Technology, Second Edition, Kluwer, Dordredcht, 1996, ch. 6, pp. 280-412 .

[6] M. Rezaei, A.F. Ismail, Gh. Bakeri, S.A. Hashemifard, and T. Matsuura, Effect of General Montmorillonite and Cloisite 15A on Structural Parameters and Performance of Mixed Matrix Membranes Contactor for CO2 Absorption, Chem. Eng. J. 2015, Vol. 260, pp. 875–885.

[7] H. Kreulen, C. A. Smolders, G. F. Versteeg, W. P. M. van Swaaij, Determination of mass transfer rates in wetted and non-wetted microporous membranes, Chem. Eng. Sci. 1993, vol. 48, pp. 2093–2102.

[8] Y. Zhang, R. Wang, Sh. Yi, L. Setiawan, X. Hu, and A. G. Fane, Novel chemical surface modification to enhance hydrophobicity of polyamide-imide (PAI) hollow fiber membranes, J. Membr. Sci. 2011, vol. 380, pp. 241– 250.

[9] P.T. Nguyen, E. Lasseuguette, Y. Médina, J.C. Remigy, D. Roizard, E. Favre, A dense membrane contactor for intensified CO2 gas/liquid absorption in post-combustion capture, J. Membr. Sci. 2011, vol. 337, pp. 261-272.

[10] Gh. Bakeri, T. Matsuura, A. F. Ismail, D. Rana, A novel surface modified polyetherimide hollow fiber membrane for gas–liquid contacting processes, Sep. Purif. Technol. 2012, vol. 89, pp. 160–170.

[11] B. Ozturk, H. B. Al-Saffar and R. Hughes, Sulphur dioxide absorption in hollow fibre membrane modules Chem. Eng. Comm. 2000, vol. 177, pp. 157-175.

[12] H. Kreulen, C. A. Smolders, G.F. Versteee and W.P.M. van Swaaij, Microporous hollow fibre membrane modules as gas liquid contactors Part 2. Mass transfer with chemical reaction, J. Membr. Sci. 1993, vol. 78, pp. 217-238.

[13] T. Papadopoulos, and K. K. Sirkar, A modified hollow fiber contained liquid membrane technique for gas separation at high pressures, J. Membr. Sci. 1994, vol. 94, pp. 163–181.

[14] D.G. Bessarabov, E.P. Jacobs, R.D. Sanderson, and I.N. Beckman, Use of nonporous polymeric flat-sheet gas-separation membranes in a membrane-liquid contactor: experimental studies J. Membr. Sci. 1996, vol. 113, pp. 275-284.

[15] D. C. Nymeijer, T. Visser, R. Assen, and M. Wessling, Composite hollow fiber gas–liquid membrane contactors , for olefin/paraffin separation, Sep. Purif. Technol. 2004, vol. 37, pp. 209–220.

[16] K. Kneifel, S. Nowak, W. Albrecht, R. Hilke, R. Just, and K.-V. Peinemann, Hollow fiber membrane contactor for air humidity control: Modules and membranes, J. Membr. Sci. 2006, vol. 276, pp. 241–251.

[17] Z. Jin, D. L. Yang, Sh. H. Zhang, and X. G. Jian, Hydrophobic modification of poly(phthalazinone ether sulfone ketone) hollow fiber membrane for vacuum membrane distillation, J. Membr. Sci. 2008, vol. 310, pp. 20–27.

[18] P.T. Nguyen, E. Lasseuguette, Y. Medina-Gonzalez, J.C. Remigy, D. Roizard, and E. Favre, A dense membrane contactor for intensified CO_2 gas/liquid absorption in post-combustion capture, J. Membr. Sci. 2011, vol. 377, pp. 261– 272.

[19] Sh. P. Yan, M. X. Fang, W. F. Zhang, Sh. Y. Wang, Zh. K. Xu, Zh. Y. Luo, and K. F. Cen, Experimental study on the separation of CO_2 from flue gas using hollow fiber membrane contactors without wetting, Fuel Process. Technol. 2007, vol. 88, pp. 501–511.

[20] W. Rongwong, R. Jiraratananona, and S. Atchariyawut, Experimental study on membrane wetting in gas–liquid membrane contacting process for CO_2 absorption by single and mixed absorbents, Sep. Purif. Technol. 2009, vol. 69, pp. 118–125.

[21] R. Faiz, and M. Al-Marzouqi, CO_2 removal from natural gas at high pressure using membrane contactors:Model validation and membrane parametric studies, J. Membr. Sci. 2010, vol. 365, pp. 232–241.

[22] J. G. Lu, Y. F. Zheng, and M. D. Cheng, Wetting mechanism in mass transfer process of hydrophobic membrane gas absorption, J. Membr. Sci. 2008, vol. 308, pp. 180–190.

[23] A.F. Ismail, A. Mansourizadeh, comparative study on the structure and performance of porous polyvinylidene fluoride and polysulfone hollow fiber membranes for CO2 absorption, J. Membr. Sci. 2010, vol. 365, pp. 319–328.

[24] Sh. Ma'mun, H. F. Svendsen, K. A. Hoff, O. Juliussen, Selection of new absorbents for carbon dioxide capture, Energy Convers. Manage. 2007, vol. 48, pp. 251–258.

[25] S. R. Wickramasinghe, M. J. Semmens, and E. L. Cussler, Mass transfer in various hollow fiber geometries, J. Membr. Sci. 1992, vol. 69, pp. 235–250.

[26] J. J. Carroll, J. D. Slupsky, and A. E. Mather. The Solubility of carbon dioxide in water at low pressure, J. Phys. Chem. Ref. Data, 1991, vol. 20, pp. 1201-1209.

[27] E. Drioli, A. Criscuoli, and E. Curcio, Membrane contactors: Fundamentals, applications and potentialities, Elsevier, Amsterdam, 2006, ch. 4, pp. 127-162.

[28] V. Y. Dindore, D. W. F. Brilman, F. H. Geuzebroek, and G. F. Versteeg, Membrane–solvent selection for CO_2 removal using membrane gas–liquid contactors, Sep. Purif. Technol. 2004, vol. 40, pp. 133–145.

[29] P.S. Kumar, J.A. Hogendoorn, P.H.M. Feron, G.F. Versteeg, Approximate solution to predict the enhancement factor for the reactive absorption of a gas in a liquid flowing through a microporous membrane hollow fiber, J. Membr. Sci. 2003, vol. 213, pp. 231–245.

[30] V. Y. Dindore, D. W. F. Brilman, P. H. M. Feron, and G. F. Versteeg, CO_2 absorption at elevated pressures using a hollow fiber membrane contactor, J. Membr. Sci. 2004, vol. 235, pp. 99–109.

[31] H. Kreulen, C. A. Smolders, G. F. Versteeg, and W. P. M. van Swaaij, Microporous hollow fiber membrane modules as gas–liquid contactor. Part 1. Physical mass transfer processes, J. Membr. Sci. 1993, vol. 78, pp. 197–216.

[32] M. Ch. Yang, and E. L. Cussler, Designing hollow-fiber contactors, AIChE Journal, 1986, vol. 32, pp.1910–1916.

[33] R. M. A. Roque-Malherbe, The Physical Chemistry of Materials: Energy and Environmental Applications, CRC press, London, 2010, ch. 5, pp. 217-271.

[34] P. Ferreira, A. Carvalho, T. R. Correia, B. P. Antunes, I. J. Correia, and P. Alves, Functionalization of polydimethylsiloxane membranes to be used in the production of voice prostheses, Sci. Technol. Adv. Mater. 2013, vol. 14, pp. 1-8.

[35] E.E. Wilson, A basis for rational design of heat transfer apparatus, Trans. ASME 1915, vol. 37, pp. 47.

[36] S. Atchariyawut, R. Jiraratananon, R. Wang, Mass transfer study and modeling of gas–liquid membrane contacting process by multistage cascade model for CO2 absorption, Sep. Purif. Technol. 2008, vol. 63, pp. 15-22.

[37] A. Mansourizadeh, A.F. Ismail, M.S. Abdullah, B.C. Ng, Preparation of polyvinylidene fluoride hollow fiber membranes for CO2 absorption using phase-inversion promoter additives, J. Membr. Sci. 2010, vol. 355, pp. 200–207.

[38] R.W. Baker, Membrane technology and applications, second edition, John Wiley & Sons, New York, 2004, ch. 8. pp. 301-353.

[39] B. E. Poling, J. M. Prausnitz, J. P. O'Connell, The Properties of Gases and Liquids, fifth edition, Boston, McGraw-Hill, 2001, ch. 8, pp. 1-193.

[40] D. A. Skoog, D. M. West, F. J. Holler, Fundamentals of analytical chemistry, sixth edition, Sunders college publishing, New York, 1992, appendix A.

[41] S. A. Hashemifard, A. F. Ismail, T. Matsuura, and N. Hilal, Predicting the structural parameters of integrally skinned porous membranes, J. Membr. Sci. 2014, vol. 454, pp. 451–462.

[42] D. L. Wang, R. X. Xu, G. L. Jiang, and B. L. Zhu, Determination of surface dense layer structure parameters of the asymmetric membrane by gas permeation method, J. Membr. Sci. 1990, vol. 52, pp. 97-108.

[43] R. B. Bird, W. E. Stewart, and E. N. Lightfoot, Transport phenomena, second ed., John Wiley & Sons, New York, 2002, ch. 1, pp. 11-39.

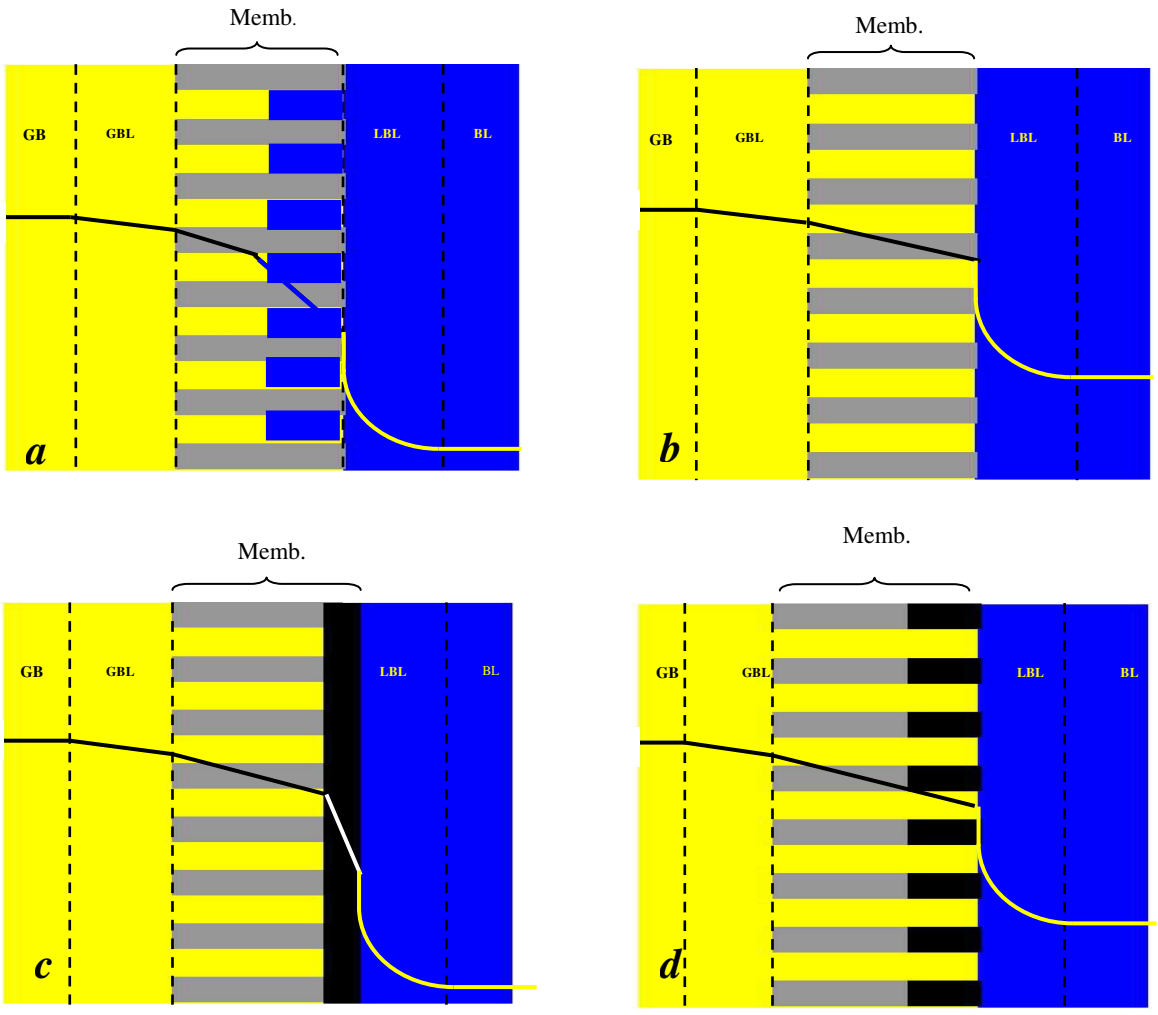

Fig. 1. a schematic of different gas/liquid contact and the concentration gradient of CO_2 in the bulk and boundary layer in gas phase, liquid phase and the membranes structure, ***a***) partially wet porous membrane contactor, ***b***) fully dry porous membrane contactor, ***c***) porous membrane contactor possessing a dense hydrophobic skin layer, ***d***) porous membrane contactor possessing a porous hydrophobic skin layer.(GB: gas bulk, GBL: gas boundary layer, LB: liquid bulk, and LBL: liquid boundary layer, and the colors represent the following media; yellow: gas stream, blue: liquid stream, gray: porous membrane cross section and black: coating layer)

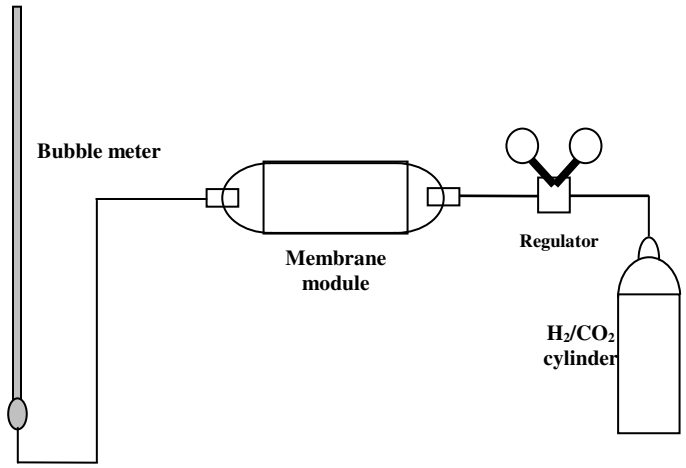

Fig. 2. Gas permeation testing rig

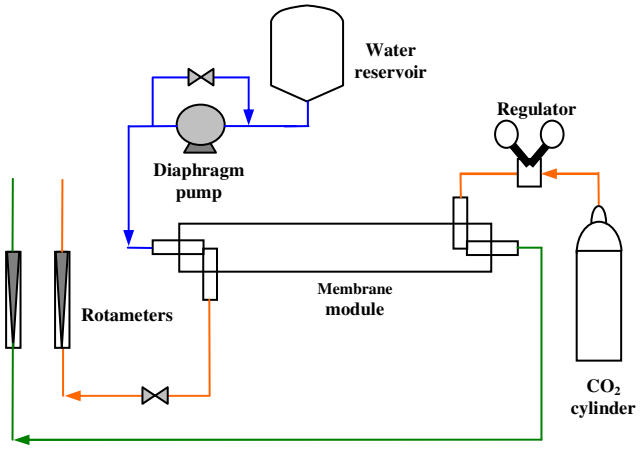

Fig. 3. Gas absorption rig (Orange: CO_2, blue: distilled water and green: CO_2 solution).

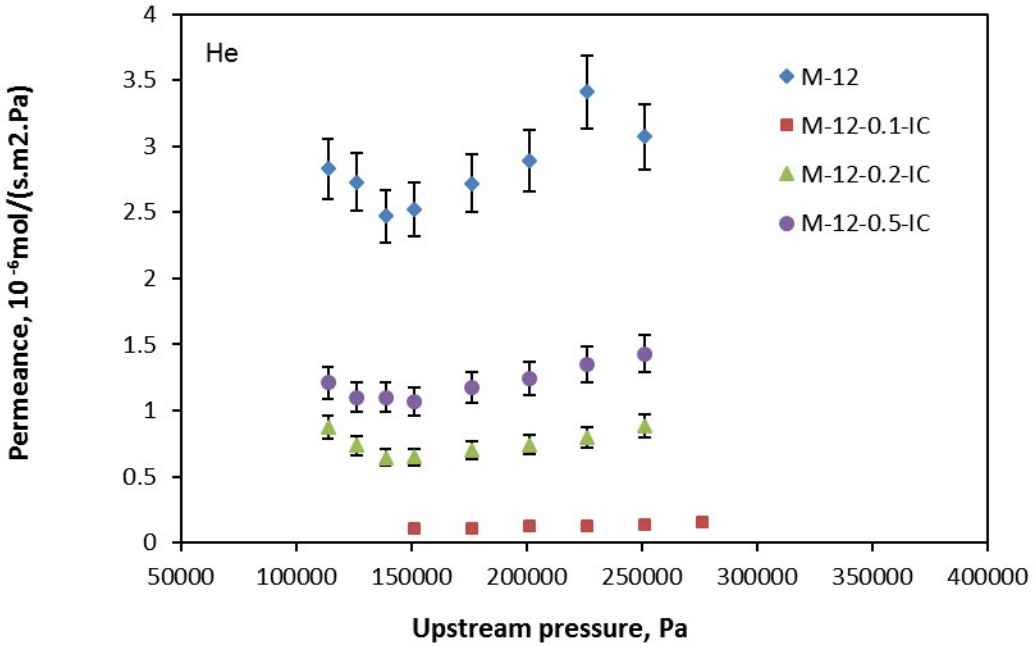

Fig. 4. Helium permeance of neat and inside silicon rubber coated PEI-12%wt hollow fiber membranes

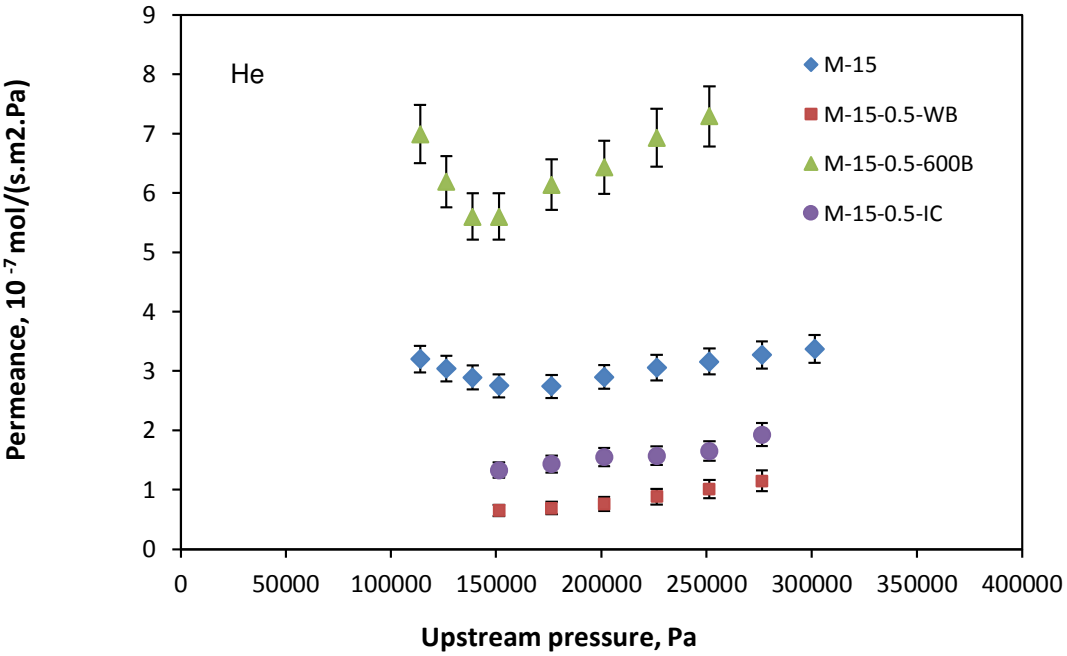

Fig. 5. Helium permeance of neat and silicon rubber coated PEI-15%wt hollow fiber membranes

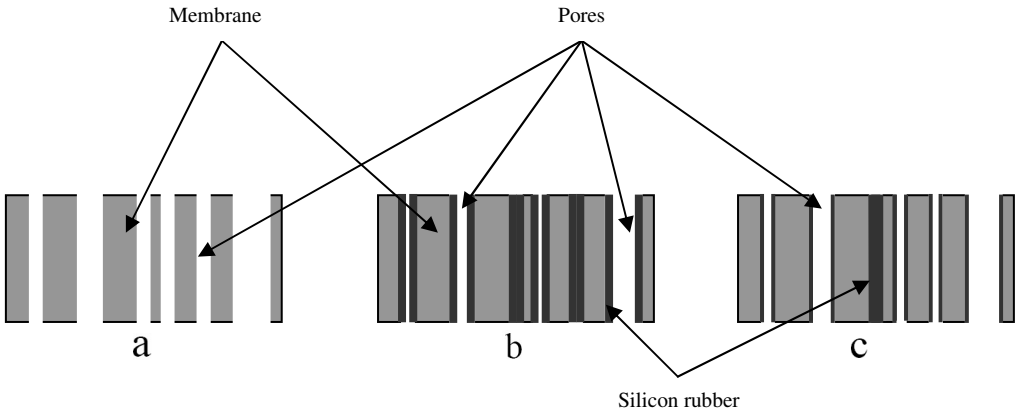

Fig. 6. Tiny and large pores in the inner skin layer of the coated and uncoated membranes at different concentration of silicon rubber solution, a) uncoated, b) 0.1 wt.% or 0.2 wt.% and, c)0.5 wt.%.(Black: Silicon rubber, Gray: Membrane matrix, White: pore channels)

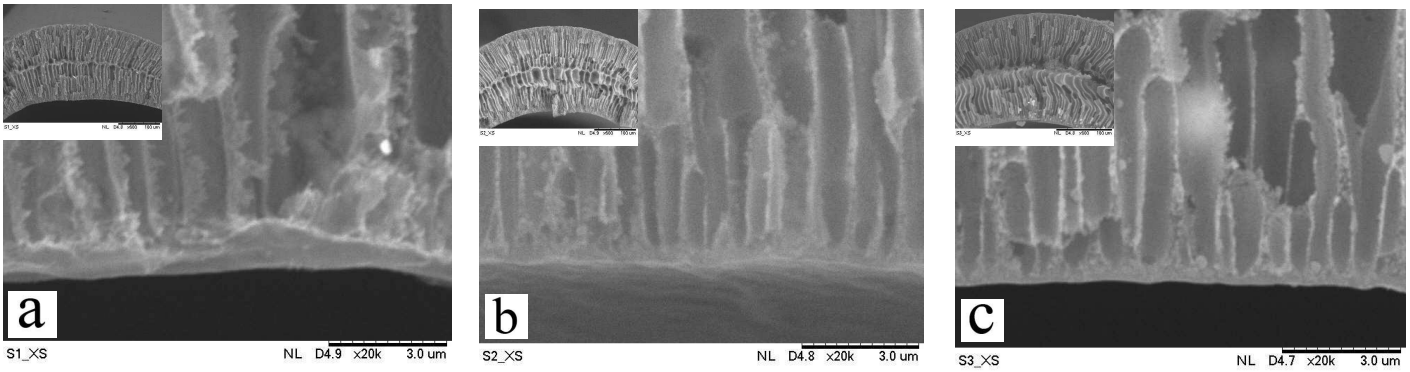

Fig. 7. SEM spectra of the cross-section and the inner coated surface of *a*) M-12-0.1-IC, *b*) M-12-0.2-IC, *c*) M-12-0.5-IC. The magnification of the top right small spectrum, from the left are X600, X600 and X800 respectively and the scale bar is 100 μm.

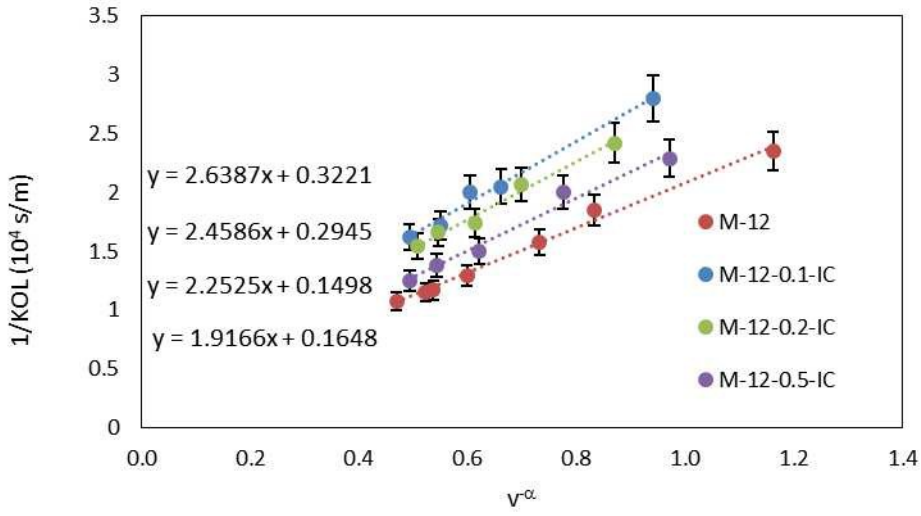

Fig. 8. Wilson plot of the fabricated membranes, effect of silicon rubber lumen side coating on the MCs overall mass transfer resistances ($\alpha \approx 0.47$)

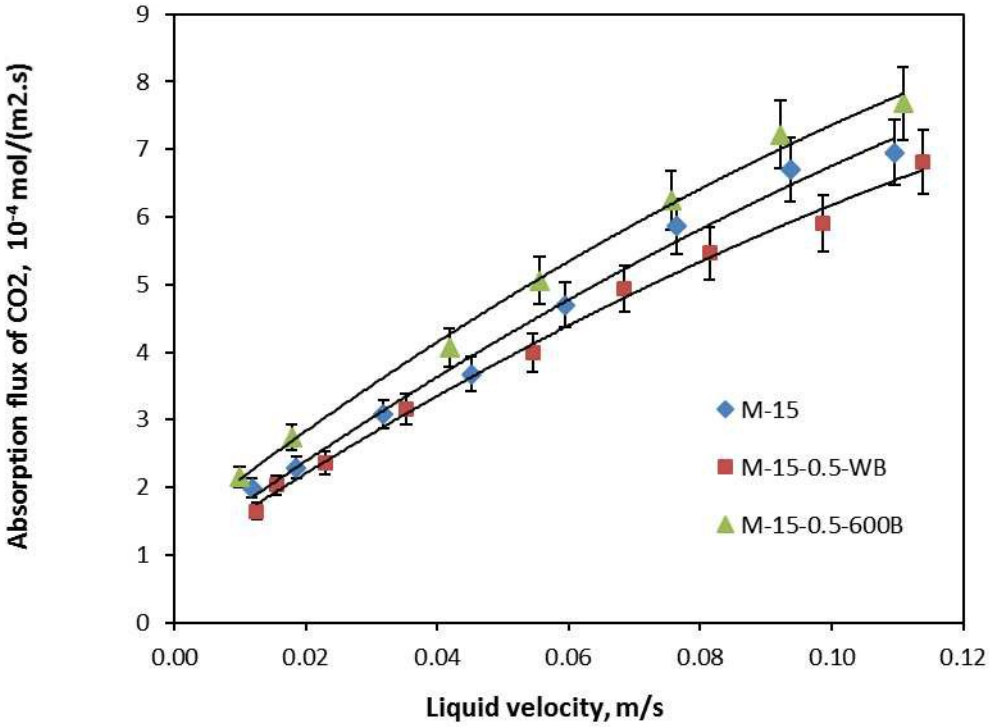

Fig. 9. CO_2 absorption flux vs. liquid velocity through shell side, effect of nitrogen blowing during the silicon rubber coating onto outside surface of the 15% PEI hollow fiber membranes on the MCs performance.

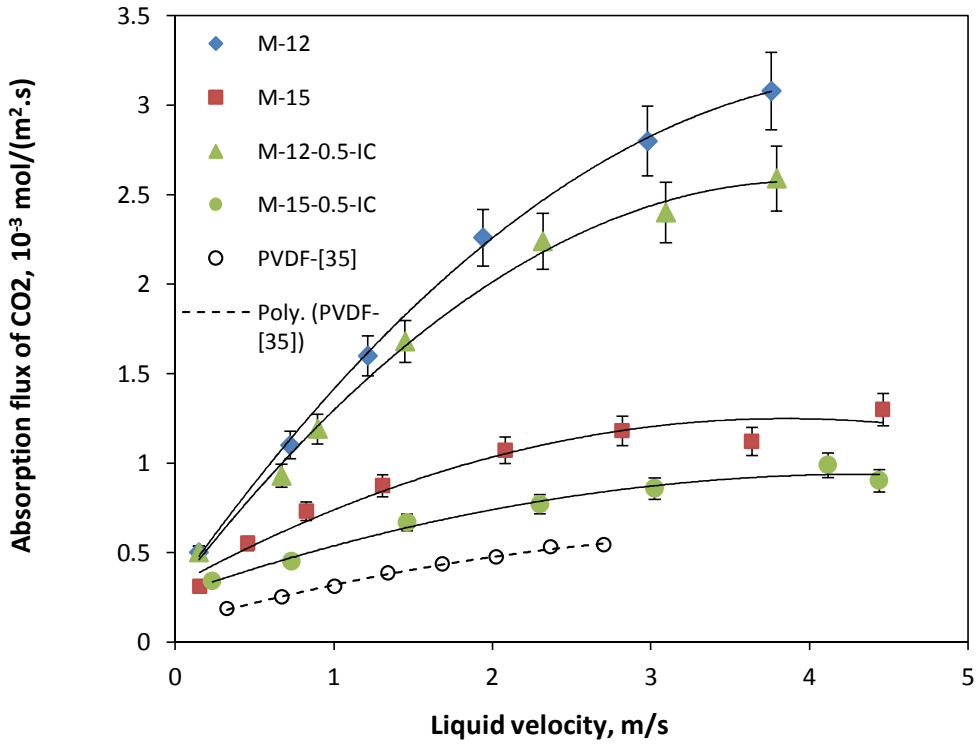

Fig. 10. CO_2 absorption flux vs. liquid velocity through lumen, effect of silicon rubber lumen side coating on the MCs performance for 15% PEI and 12%PEI hollow fibers.

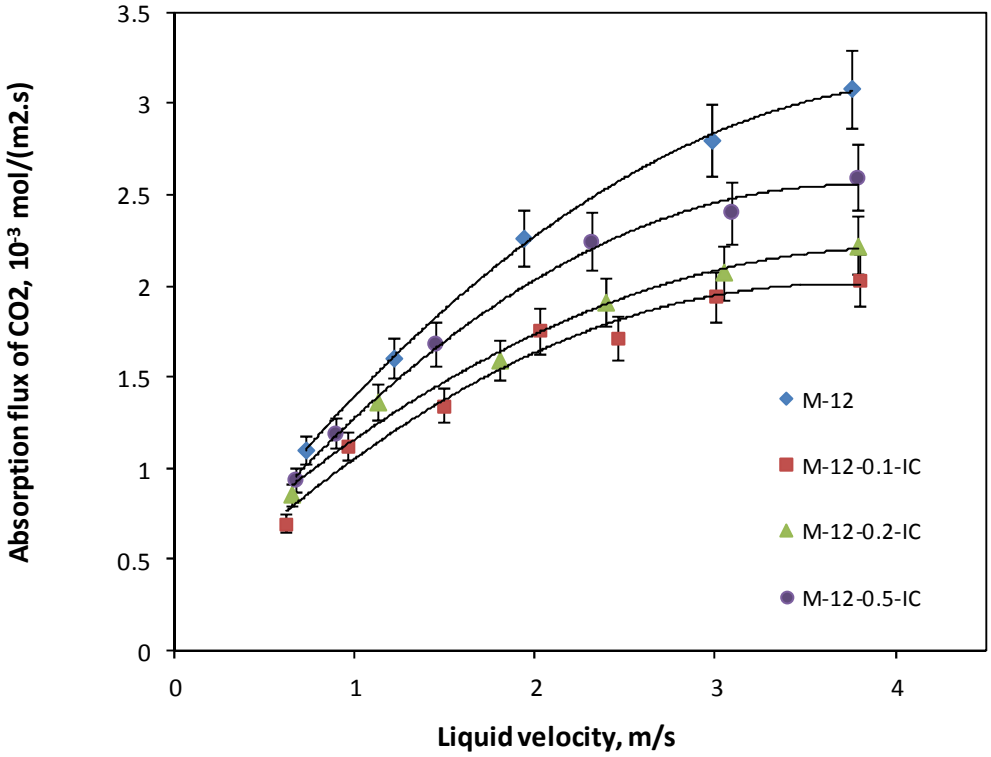

Fig. 11. CO_2 absorption flux vs. liquid velocity through lumen, effect of silicon rubber concentration on the MCs performance for 12 wt% PEI hollow fibers.

Table 1. A brief review on the coating of hollow fiber membrane for gas/liquid contactor

Researcher	Polymer	Membrane Config.	Coating layer	Coated layer structure	Absorbent	Application	Ref.
Kreulen et al. (1993)	PP	Hollow fiber	PDMS	Dense	Sodium hydroxide	CO_2 and N_2O	[10]
Papadopoulos and Sirkar (1994)	PP	Hollow fiber	PDMS	Dense	Water and DEA	CO_2/N_2	[11]
Bessarabov et al. (1996)	PDMS	Dense flat sheet	-	Dense	Water	CO2	[12]
Nymeijer et al. (2004)	PP Accurel®	Hollow fiber	EPDM	Dense	$AgNO_3$ solutions	C_2H_6/C_2H_4	[13]
Kneifel et al. (2006)	PEI	Hollow fiber	PDMS	Dense	Water	Air humidity	[14]
Jin et al. (2008)	PPESK	Hollow fiber	PDMS	Dense	Water	Water vapour	[15]
Nguyen et al. (2011)	PP Oxyphan®	Hollow fiber	PTMSP or Teflon AF2400	Dense	MEA	CO_2	[16]

All of the abbreviations are defined in the text

Table 2. Code and specifications of the fabricated membranes before and after coating

Membrane code	PEI concentration wt.%	Silicon rubber wt.%	Coated surface	Remark
M-15	15	-	-	Uncoated
M-15-0.5-WB	15	0.5	Outside	Without N2-Blowing
M-15-0.5-600B	15	0.5	Outside	600 kPa N2-Blowing
M-15-0.5-IC	15	0.5	Inside	N2-Blowing
M-12	12	-	-	Uncoated
M-12-0.1-IC	12	0.1	Inside	N2-Blowing
M-12-0.2-IC	12	0.2	Inside	N2-Blowing
M-12-0.5-IC	12	0.5	Inside	N2-Blowing

Table 3. Prediction of pore size and effective surface porosity by Partial slip model (ψ=0.5), using helium as probe gas at room temperature.

Membrane	r_p(nm)	ε/l_p(m^{-1})
M-12	193±10	66.5±10
M-12-0.1-IC	332±40	5.91±0.6
M-12-0.2-IC	290±40	9.94±1.5
M-12-0.5-IC	240±15	21.7±12
M-15	148±10	9.7±2.0
M-15-0.5-IC	228±10	2.8±0.5
M-15-0.5-WB	864±60	0.17±0.04
M-15-0.5-600B	278±30	9.15±0.8

Table 4. Contact angle and CEPw of the coated and uncoated hollow fiber membranes.

Membrane code	Contact angle(°)	CEPw (kPa)
Dense PDMS	106*	-
M-15	82±1.4	800±50
M-15-0.5-WB	111±2.9	800±50
M-15-0.5-600B	114±2.2	900±50
M-15-0.5-IC	115±2	1000±50
M-12	78±3.4	300±50
M-12-0.1-IC	108±4.5	550±50
M-12-0.2-IC	116±1.7	600±50
M-12-0.5-IC	114±3.4	600±50

*From reference [34]

Table 5. Comparison between membrane mass transfer resistances based on gas absorption results and gas permeation results.

Membrane code	Gas absorption approach (Wilson plot)				Gas permeation approach				
	R_{OL} (s/m)	R_L (s/m)	R_M (s/m)	k_M (10^{-4} m/s)	r_p (nm)	ε/l_p (m^{-1})	D_G (10^{-5} m^2/s)	R_M (s/m)	k_M (10^{-4} m/s)

M-12	11708±1100	10087	1621	4.75	193±10	66.5±10	1.2	374	8.01
M-12-0.1-IC	17175±1300	13970	3205	1.54	332±40	5.91±0.6	1.34	3712	0.81
M-12-0.2-IC	16556±1100	13622	2934	1.66	290±40	9.94±1.5	1.31	2293	1.31
M-12-0.5-IC	13831±1200	12337	1494	7.29	240±15	21.7±12	1.27	1090	2.75

Table 6. The effect of silicon rubber coating on the helium GPT results and carbon dioxide absorption flux.

Membrane code	$(\varepsilon/lp)/(\varepsilon/lp)_{M\text{-}12}$	$P/P_{M\text{-}12}$	$J/J_{M\text{-}12}$ (v =3.0 m/s)
M-12-0.1-IC	0.014±0.001	0.041±0.003	0.669±0.074
M-12-0.2-IC	0.150±0.020	0.265±0.033	0.633±0.058
M-12-0.5-IC	0.326±0.042	0.428±0.060	0.825±0.069